3832 *Chem. Mater.* **2010,** *22,* 3832–3842
DOI:10.1021/cm902316p

CHEMISTRY OF MATERIALS
Article

Understanding the Supramolecular Self-Assembly of Zirconium Titanate Mesophases Formed from the Poly(ethylene oxide) Surfactant Brij-58

Vittorio Luca,* Elizabeth Drabarek, Christopher. S. Griffith, and Tracey L. Hanley

Australian Nuclear Science and Technology Organisation, Institute of Materials Engineering, New Illawarra Road, Lucas Heights, NSW 2234, Australia

Received July 28, 2009. Revised Manuscript Received May 18, 2010

The evaporation-induced self-assembly of mesoporous zirconium titanium oxide thin films prepared from precursor solutions with the composition $Zr_xTi_{1-x}Cl_4$:40 EtOH:0.005 Brij 58:*h* H_2O (where $x = 0.28$, $h = 10$, and Brij 58 = diblock copolymer $C_{16}H_{33}PEO_{20}$) by dip coating has been studied as a function of the mole fraction of zirconium (x), the relative humidity (RH), and the drying conditions. Extremely well-ordered mesophases and compositional homogeneity on the atomic scale were consistently obtained when the films were prepared at relative humidities above 60%, under which conditions a cubic phase was identified. The influence of humidity was monitored using a combination of in situ small-angle X-ray diffraction (SAXD) and small-angle X-ray scattering (SAXS). These techniques showed the existence of nanocrystalline phases during the initial drying process for films prepared from precursor solutions with x in the range of 0.20−0.60. The nanocrystalline phases were evidenced as multiple X-ray reflections above 8° 2θ. These reflections were ascribed to relatively crystalline nano building units of the mesophase and displayed only a transient stability in humid air, disappearing after ∼1 h of film conditioning in any humidity. A clear dependence of the primary *d*-spacing observed in the SAXD on composition for films dried at 65% RH, stabilized at 200 °C, and calcined at 350 °C provided strong evidence of the ability to form a complete solid solution of Zr and Ti in the oxide mesophase prepared from the precursor solutions. This compositional homogeneity was confirmed by transmission electron microscopy and further corroborated using Ti *K*-edge X-ray absorption spectroscopy, which probed the local chemical environment of the embedded Ti atoms. The data provided here are in stark contrast to studies of zirconium titanium mixed oxide film systems using similar preparation procedures but triblock copolymer porogens such as F-127. A hypothesis is tendered to explain the dramatic difference in the products obtained using these distinct but related copolymer templates.

Introduction

Mesoporous metal oxides prepared through supramolecular self-assembly have been intensively studied, because they potentially have many applications. However, there have so far been relatively few areas in which the performance of these materials has surpassed that of conventional materials. We are interested in the development of materials with applications in separations, in particular, within the context of the nuclear industry. In this regard, Fryxell et al.[1] and other researchers[2] have demonstrated how the internal surfaces of mesoporous silicates can be functionalized with bifunctional organic molecules to impart selectivity for the adsorption of nonradioactive heavy metals. This was subsequently extended to radio-lanthanides[3] and actinides.[4] There is now a large body of research devoted to the functionalization of mesoporous silicates, and the field has recently been reviewed comprehensively.[5]

In contrast to much of the previous work, the focus of our program of investigation has been the development of mesoporous mixed zirconium titanium oxides for applications as adsorbents in the context of nuclear waste management. One potential advantage of focusing on mixed zirconium titanium oxides is the ability to convert the spent adsorbents directly to dense and highly durable zirconium titanate ceramics such as zirconolite, within whose structure the radio nuclides are locked.[6] Alternatively, the same radionuclide-loaded adsorbents could be used as inert matrix fuels. Flexibility in the composition of the inert matrix is important to enable tailoring of the neutronics of either targets or fuels. In this regard, thermally stable zirconium titanium oxide xerogels with disordered wormhole

*Author to whom correspondence should be addressed. Tel.: 54-11-6772 7018. E-mail: vluca@cnea.gov.ar. Web: www.cnea.gov.ar.

(1) Feng, X.; Fryxell, G. E.; Wang, L.-Q.; Kim, A. Y.; Liu, J.; Kemner, K. M. *Science* **1997**, *276*, 923.
(2) Mercier, L.; Pinnavaia, T. J. *Environ. Sci. Technol.* **1998**, *32*, 2749.
(3) Fryxell, G. E.; Wu, H.; Lin, Y. H.; Shaw, W. J.; Birnbaum, J. C.; Linehan, J. C.; Nie, Z. M.; Kemner, K.; Kelly, S. *J. Mater. Chem.* **2004**, *14*, 3356.
(4) Fryxell, G. E.; Lin, Y.; Fishkum, S.; Birnbaum, J. C.; Wu, H.; Kemner, K.; Kelly, S. *Environ. Sci. Technol.* **2005**, *39*, 1324.
(5) Hoffmann, F.; Cornelius, M.; Morell, J.; Froba, M. *Angew. Chem., Int. Ed.* **2006**, *45*, 3216.
(6) Luca, V.; Bertram, W. K.; Widjaja, J.; Mitchell, D. R. G.; Griffith, C. S.; Drabarek, E. *Microporous Mesoporous Mater.* **2007**, *103*, 123.

Published on Web 06/09/2010

mesoporous textures have been prepared[6] and the adsorption properties of such xerogels have been investigated in detail.[7] The preparation and adsorption properties of mesoporous beads of similar composition that are suitable for large-scale column chromatographic application have also been described.[8] From these investigations, we have demonstrated the preparation of zirconium titanium mixed oxide materials with hierarchical porosity in the form of robust beads. As a result of their hierarchical porosity, these materials showed enhanced mass-transfer kinetics, relative to mesoporous materials with monomodal porosity. Rapid adsorption kinetics are highly desirable in nuclear and other applications.

Recently, the preparation of bulk large mesoporous zirconium titanates, with $Zr/(Zr + Ti) = 0.3$, using the triblock copolymer F-127 as the porogen, has been addressed.[9] In the $TiCl_4$−block copolymer−EtOH−H_2O system, as in many others, the relative humidity (RH) of the drying environment has been identified as a critical parameter. However, it was determined that the humidities necessary to afford order (> 25% RH) in this particular mixed oxide system were not conducive to also generating compositional homogeneity and high surface areas; instead, phase segregation at low temperatures was observed. The consequence of this phase segregation was poor thermal stability and subsequent crystallization of TiO_2 and ZrO_2. Conversely, at low humidities, compositional homogeneity and high surface areas could be achieved, but at the expense of order. Therefore, the preparation of ordered, compositionally homogeneous zirconium titanium mixed oxides with large mesopores remains a challenge.

Regardless of the degree of structural order, tailorability of the pore architecture and dimensions is extremely desirable; this would allow the material and its properties to be tuned to a particular application. Accessibility of cation binding sites in unfunctionalized and functionalized mesoporous silicates has been addressed, and, generally, slow kinetics have so far been observed with larger pore materials ostensibly identified as having somewhat superior mass-transport properties.[10−12] Beyond the pore architecture, in adsorption applications, it is also important to be able to prepare bulk materials in a form suitable for large-scale ion exchange applications (e.g., as millimeter-sized beads). However, the development of such materials requires a thorough understanding of the synthesis mechanism of the particular amphiphile−metal-oxide system.

It is well-known that the final state (phase or architecture) of a macromolecular system is dependent on many factors, including the initial surfactant and precursor chemistry (composition), as well as the temperature and volume fraction (f) of the assembling molecules. Variation in f is perhaps one of the most studied variables in attempts to alter the phase chemistry for simple binary block copolymer systems composed of a macromolecule and a single solvent. It is well-known that different surfactant morphologies can be "frozen in" kinetically by employing different evaporation rates during the preparation of cast films.[13,14] The self-assembly of metal oxides using block copolymers is far more complex than a simple block copolymer−solvent system, because of the introduction of molecular metal precursors that are not simply passive components. The metal precursors do not just interact with both solvent and the block copolymers themselves; they simultaneously polymerize in the presence of water over time, such that the system itself is constantly evolving, even if all else is held constant. Hence, in the so-called evaporation-induced self-assembly (EISA), where f changes as solvent is lost by evaporation (in similar fashion to increasing the concentration in block copolymer−surfactant systems), it has been shown very clearly how important control of this parameter can be.[15] In the EISA paradigm, several additional synthetic parameters can also be considered to be crucial in determining whether a mesophase forms and what amount of structural order is obtained.[16] In the case of titanate systems, highly acidic conditions are employed to catalyze hydrolysis while, at the same time, arresting or retarding condensation.

A certain level of understanding of the reaction mechanism involved in EISA thin films of both silicate and titanate has now been achieved and reviewed.[17] However, relatively little is known concerning the self-assembly of mixed-metal-oxide systems that have the potential to be correspondingly more complex.

Paradoxically, the behavior of even the relatively simple ternary systems of some of the most studied metal-oxide−block-copolymer systems (F-127, P-123, and Brij 58) are not that well-understood and continue to be actively studied. For instance, relatively recently, Holmqvist et al.[18] reported the behavior of the F-127−alkanol−water system and have described a rich phase behavior. Soni et al.[19] have only just recently investigated the P-123−ethanol−water phase diagram. The B58−alkanol−water ternary phase diagram has not been investigated, although the B58−water binary system was studied in the late 1980s.[20]

(7) Griffith, C. S.; Sizgek, G. D.; Sizgek, E.; Scales, N.; Yee, P. J.; Luca, V. *Langmuir* **2008**, *24*, 12312.
(8) Sizgek, G. D.; Sizgek, E.; Griffith, C. S.; Luca, V. *Langmuir* **2008**, *24*, 12323.
(9) Luca, V.; Soler-Illia, G. J. de A. A.; Angelome, P. C.; Steinberg, P. Y.; Drabarek, E.; Hanley, T. L. *Microporous Mesoporous Mater.* **2009**, *118*, 443.
(10) Walcarius, A.; Delacote, C. *Chem. Mater.* **2003**, *15*, 4181.
(11) Walcarius, A.; Etienne, M.; Lebeau, B. *Chem. Mater.* **2003**, *15*, 2161.
(12) Walcarius, A.; Etienne, M.; Bessiere, J. *Chem. Mater.* **2002**, *14*, 2757.
(13) Huang, H.; Zhang, F.; Hu, Z.; Du, B.; He, T. *Macromolecules* **2003**, *36*, 4084.
(14) Kim, G.; Libera, M. *Macromolecules* **1998**, *31*, 2569.
(15) Cagnol, F.; Grosso, D.; Soler-Illia, G. J. de A. A.; Crepaldi, E. L.; Babonneau, F.; Amenitsch, H.; Sanchez, C. *J. Mater. Chem.* **2003**, *13*, 61.
(16) Brinker, C. J.; Lu, Y.; Sellinger, A.; Fan, H. *Adv. Mater.* **1999**, *11*, 579.
(17) Grosso, D.; Cagnol, F.; Soler-Illia, G. J. de A. A.; Crepaldi, E. L.; Amenitsch, H.; Brunet-Bruneau, A.; Bourgeois, A.; Sanchez, C. *Adv. Func. Mater.* **2004**, *14*, 309.
(18) Holmqvist, P.; Alexandridis, P.; Lindman, B. *Langmuir* **1997**, *13*, 2471.
(19) Soni, S. S.; Brotons, G.; Bellour, M.; Narayanan, T.; Gibaud, A. *J. Phys. Chem. B* **2006**, *110*, 15157.

The objectives of the present study were 2-fold: (1) to prepare compositionally homogeneous and highly ordered mesoporous zirconium titanium oxide mesophase thin films, using the classical block copolymer surfactant Brij 58 (B58), and (2) to provide some understanding of the synthesis mechanism of this mixed-oxide mesophase system. In pursuing this latter objective, both ex situ and in situ small-angle X-ray scattering (SAXS) and small-angle X-ray diffraction (SAXD) were used.

Experimental Section

Sample Preparations. All films in this study were prepared by dip coating according to the method of Crepaldi et al.,[21] using only a precursor solution with the composition a $ZrCl_4$:b $TiCl_4$:40 EtOH:0.05 B58:20 H_2O, where B58 is $C_{16}H_{33}PEO_{20}$. The mole fraction of zirconium in this precursor solution is represented by x ($x = a/(a + b)$) and was varied over a range of $x = 0-1$, in increments of 0.2. The products are referenced using the nomenclature B58-ZrTi-x. Dip coating was conducted in a Perspex chamber in which the RH value was controlled and then monitored using a Vaisala Model HMI41 probe.

Ex Situ X-ray Diffraction. For ex situ X-ray diffraction (XRD) studies, the mesophase films were prepared in a dipping chamber remote from the diffractometer. The humidity in the dipping chamber was fixed at ~50%−60%, depending on the requirements, and was monitored using a calibrated Vaisala Model HMI41 humidity probe. As soon as the films had been drawn at the specified humidity ($T = 0$), they were enclosed in an airtight jar and transported into a constant-humidity chamber that was attached to a Scintag Model X1 diffractometer, where the recording of the pattern commenced in $\theta-\theta$ geometry. The humidity in the chamber was controlled using a commercial humidity controller and also was monitored throughout the experiment. Ten minutes were requried to record the first pattern; thereafter, patterns were obtained every 9 min, separated by an interval of 30 s.

In Situ Small-Angle X-ray Scattering. In situ small-angle X-ray scattering (SAXS) was conducted using the experimental setup depicted in Figure 1. Because of the need to record samples in a vacuum chamber, an aged precursor solution was loaded into a capillary sitting in the vertical orientation using a peristaltic pump that was fed by a constant atmosphere from a humidity control apparatus. The constant-RH air feed to the pump was monitored continuously in a mixing chamber position just ahead of the pump inlet. The empty capillary background was taken prior to any data acquisition.

The protocol for these in situ experiments consisted of the precursor solution being drawn into a 2-mm capillary located in the beam path without being irradiated. The precursor solution was then flushed from the capillary by the air flow with a controlled RH value from a peristaltic pump, which produced an air flow of 8.5 mL/min. Immediately upon emptying the capillary ($T = 0$), the X-ray shutter was opened and data was continuously taken every 100 s. Typically, 100 s were needed to totally flush the capillary of excess precursor solution and commence the drying process. The precursor solutions were measured independently, using a filled and sealed 2-mm quartz capillary.

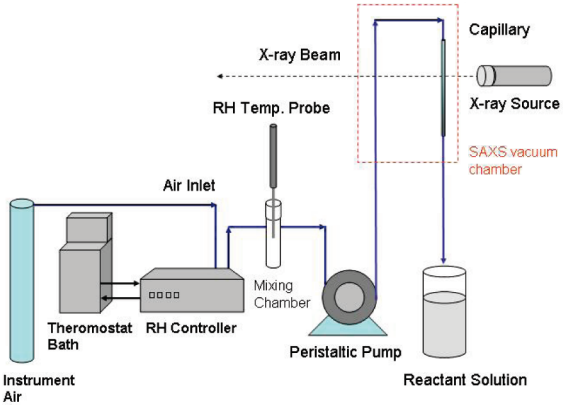

Figure 1. Experimental setup used for in situ small-angle X-ray scattering (SAXS) experiments.

SAXS measurements were performed on a Bruker Model Nanostar SAXS camera, with pinhole collimation for point focus geometry. The instrument source was a copper rotating anode (0.1 mm filament) operating at 50 kV and 24 mA, fitted with cross-coupled Göbel mirrors, resulting in Cu Kα radiation with a wavelength of 1.54 Å. The SAXS camera was fitted with a Hi-star 2D detector (effective pixel size = 100 μm). The sample-to-detector distance was chosen to be 300 mm, which provided a q-range of 0.03−0.69 Å^{-1} ($q = (4\pi \sin \theta)/\lambda$, where θ is the scattering angle and λ is the wavelength of the incident X-rays).

Transmission Electron Microscopy. Transmission electron microscopy (TEM) was conducted using a JEOL Model 2000FXII instrument operated at an acceleration potential of 200 keV. The mixed-oxide thin films were scraped off the glass slides and ground to fine powders. The powders were then dispersed in methanol and sonicated for 20 min. One drop of suspension was applied to the surface of a holey carbon-coated grid.

X-ray Absorption Fine Structure. Room-temperature transmission X-ray absorption fine structure (EXAFS) spectra were recorded at the Ti K-edge on beamline 20B at the Photon Factory, Tsukuba, Japan, using a Si(111) double monochromator. An estimate of the resolution ($\Delta E/E$) was calculated from the Darwin width of the Si(111) monochromator and the slit opening of 0.4 mm; a value of 1.36 eV was obtained.[22] This value was very similar to the peak-to-peak first derivative line width obtained for a Ti foil reference spectrum. Samples were scraped off the glass substrates and diluted by mixing boron nitride and then loaded into sample holders with Kapton windows. Calibration of the energy scale was performed using a Ti foil placed between the second and third ion chambers. In some cases, weak signals from the reference foil made accurate establishment of the energy threshold difficult.

The films were removed from the glass substrates using a blade. To avoid thickness effects, scrapings were diluted and thoroughly mixed with boron nitride. Analysis of the EXAFS was performed with the program XFIT.[8] Backscattering amplitude and phase shifts were calculated ab initio, using the single scattering theory implemented within the FEFF4 code. Fitting was performed in R-space, since it is generally considered to be advantageous.[23] Initial values of the energy zero (E_0) and the amplitude reduction factor (S_0^2) were obtained by fitting the EXAFS of a crystalline anatase reference sample with the

(20) Schefer, J.; McDaniel, R.; Schoenbomt, B. P. *J. Phys. Chem.* **1988**, *92*, 729.
(21) Crepaldi, E. L.; Soler-Illia, G. J. de A. A.; Grosso, D.; Sanchez, M. *New J. Chem.* **2003**, *27*, 9.
(22) Luca, V.; Djajanti, S.; Howe, R. F. *J. Phys. Chem. B* **1998**, *102*, 10650.
(23) Koningsberger, D. C.; Mojet, B. L.; Van Dorssen, G. E.; Ramaker, D. E. *Top. Catal.* **2000**, *10*, 143.

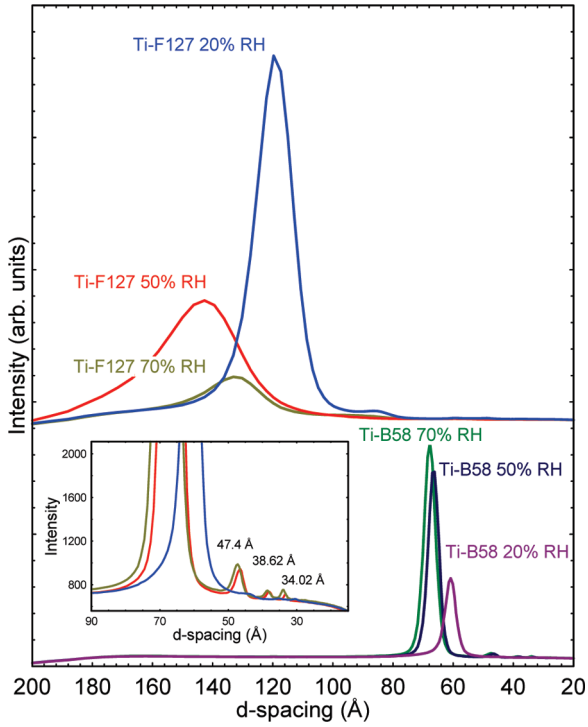

Figure 2. Small-angle diffraction pattern (transmission mode) of B58-ZrTi-*0* and F127-ZrTi-*0* films prepared at 20%, 50%, and 70% RH. Data recorded in the 90° orientation for films deposited on glass wafers.

number of nearest-neighbor atoms (N), their distance (R), and the Debye−Waller factor (σ^2) fixed at their expected crystallographic values and allowing E_0 and S_0^2 to float simultaneously. The obtained values of E_0 and S_0^2 were then used as initial values for the modeling of the less-crystalline samples.

Results

Characterization by Ex Situ Diffraction. In the present study, the main focus was on the preparation of B58-ZrTi-x thin films with a range of x values. As a preliminary step, low-angle diffraction patterns of B58-ZrTi-0 films (on borosilicate glass substrates) prepared ex situ at 20%, 50%, and 70% RH and stabilized at 200 °C were recorded at a synchrotron X-ray beamline in a 90° orientation (see Figure 2). Several months elapsed between the preparation of these films and their examination. Up to four reflections were observed for each of the three films with primary reflections at 60, 66.9, and 67.9 Å for samples prepared at 20%, 50%, and 70% RH, respectively. As the humidity during film preparation was increased, the intensity of the primary reflection also increased, suggesting that higher humidities during film formation favored ordering. For the most-well-ordered B58-ZrTi-*0* films prepared at 70% RH, the higher-angle reflections were observed at 47.4, 38.6, and 34.02 Å. These are consistent with a cubic unit cell, for which the expected d-spacings would be 48.0 (200), 39.2 (211), and 34.0 Å (220). This observation is contrary to previous reports of mesophase films prepared from $TiCl_4$ and B58 (using procedures

(24) Grosso, D.; Babonneau, F.; Sanchez, C.; Soler-Illia, G. J. de A. A.; Crepaldi, E. L.; Albouy, P. A.; Amenitsch, H.; Balkenende, A. R.; Brunet-Bruneau, A. *J. Sol−Gel Sci. Technol.* **2003**, *26*, 561.

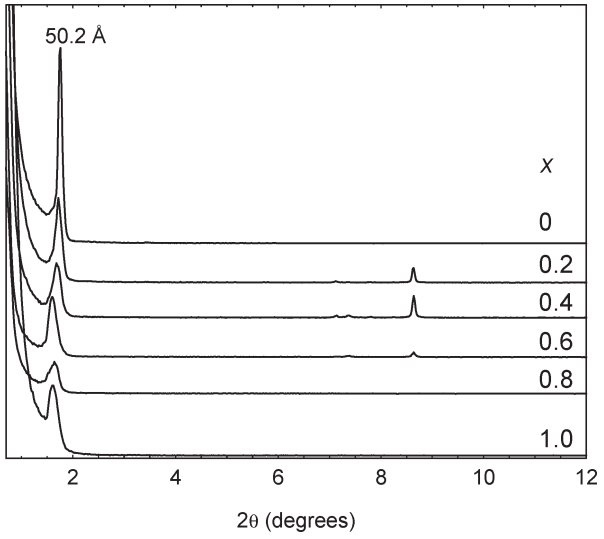

Figure 3. Compositional (x) dependence of the low-angle diffraction pattern (reflection mode) of B58-ZrT-x films prepared at 65% RH. The mole fraction of Zr (x) is given above each pattern.

similar to those used here), which were assigned to a two-dimensional (2D) hexagonal ($P6m$) space group.[24] The increase in scattering intensity of the primary reflection, as a function of the relative humidity, suggests that the mesopore order of the materials increased as the humidity increased. In previous studies of the related $TiCl_4$−F-127−EtOH−H_2O system, it had been concluded that humidities of > 50% provided superior order. Therefore, further experiments were conducted at humidities above ~60% RH. For comparison with the B58-ZrTi-0 films, identically prepared and treated films of F127-ZrTi-*0* are also provided in Figure 2. Much broader reflections were obtained in all cases for these triblock copolymer-derived thin films, suggesting that greater order is a general feature of the B58 surfactant system.

To explore variations in film structure as a function of composition, thin films were prepared from precursor solutions that had different values of x. The B58-ZrTi-x films were drawn in a dipping chamber, where the dipping speed and the humidity could be precisely controlled and monitored. Low-angle XRD patterns of these films with increasing x prepared at 65% RH and conditioned at the same humidity for several days were recorded in reflection mode on a diffractometer using $\theta-\theta$ geometry. For the B58-ZrTi-*0* film, a single low-angle reflection was observed with a d-spacing of 50.2 Å, and this shifted to lower angles in a linear fashion as the Zr content increased (see Figure 3). For samples with $0.2 \leq x \leq 0.8$, several sharp high-angle reflections located between ~6°−9° 2θ were also observed. The most intense of these high-angle reflections had a d-spacing of ~12 Å (see Figure S1 in the Supporting Information). It is surmised that such high-angle reflections are attributable either to nanocrystalline building blocks of the mesophase or that they are present along with the mesophase in the precursor solution. Similar features, although with slightly different d-spacings, that similarly disappeared on aging were directly observed in several past studies of mesophase formation

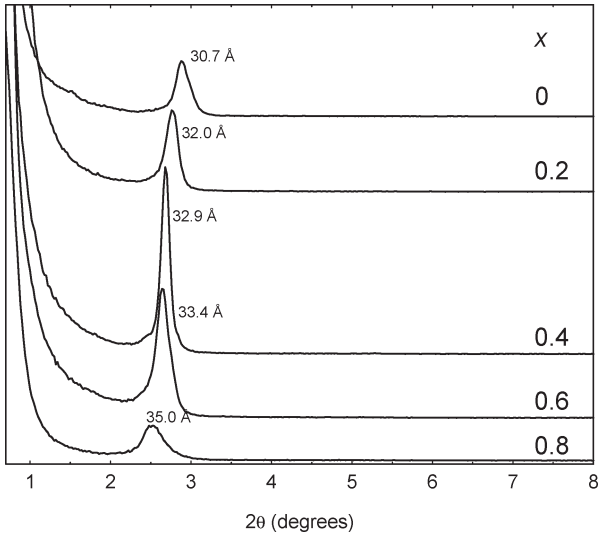

Figure 4. Compositional (x) dependence of the low-angle diffraction pattern (reflection mode) of B58-ZrTi-x films prepared at 65% RH and stabilized at 200 °C.

in titanium oxide−surfactant systems and were assigned to $Ti_wO_x(OH)_yOEt_z$ nanoclusters.[25] Sharp reflections that similarly disappear on aging were also observed in our previous work.[26] Recently, in SAXS investigations of the F-127−TiO_2 system, broad correlation peaks with similar d-spacings were observed and attributed to scatter from partially crystalline building units.[27]

In the ex situ diffraction laboratory-based experiments, it was generally found that the humidity in the dipping chamber had to exceed 65% RH to achieve a strong initial low-angle mesophase reflection, irrespective of the humidity used during subsequent conditioning, following the initial drying (see Figure S2 in the Supporting Information). The term "conditioning" is used here to indicate the curing of the film in an atmosphere of fixed humidity that occurred more than 10 min after the initial film deposition step. On the other hand, when the humidity during film preparation was increased to 98%, very poorly ordered mesostructures were also observed (see Figure S3 in the Supporting Information).

Dehydration of the B58-ZrTi-x film samples prepared at 65% RH, conditioned at similar humidities, and then stabilized at 200 °C generated the diffraction patterns shown in Figure 4. For these heated samples, the d-spacing of the low-angle reflection moved systematically to lower diffraction angles as the Zr content increased, and the plot of d-spacing as a function of x (Figure 5) was linear, as was the case for the unheated samples. This result suggests that the incorporation of Zr results in a corresponding enlargement of the unit cell. In other words, the present mesophase films consist of a complete solid solution of zirconium and titanium. Each of the structures obtained as a function of increasing x can be assigned to a cubic

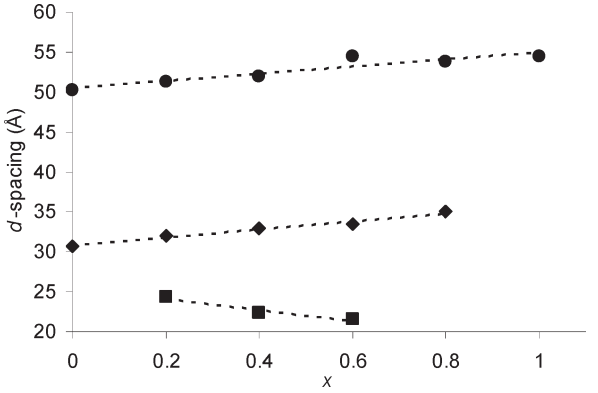

Figure 5. Variation in d-spacing with x for B58-ZrTi-x films (●) prepared at 65% RH, (◆) stabilized at 200 °C, (■) and calcined at 350 °C.

mesophase; the only differences were a progressive change in the position, intensity, and breadth of the low-angle reflections without the introduction of any additional features. When the samples were further heated to 350 °C, it was evident from Figure 5 that the linear trend in d-spacing, as a function of x, was reversed. That is, the unit cell shrinks with increasing Zr content.

The B58-ZrTi-0.4 films displayed the greatest intensity of the nanocrystal peaks; hence, it was chosen for more-detailed study of the role of these nanocrystal moieties in the self-assembly process. Experiments were designed to monitor the evolution of the diffraction pattern with time. Immediately following the dipping process, the film was enclosed in an airtight jar and transported to a diffractometer equipped with a purpose-built humidity chamber. The time from initial dipping to acquisition of the first pattern was 10 min.

Figure 6 shows that, as the time from dipping was increased, the sharp high-angle reflections (ca. 6°−9° 2θ) were reduced in intensity, while the low-angle reflections (ca. $<3°$ 2θ) underwent a corresponding slight increase in intensity. This is highlighted when the integrated intensities of these two features are plotted as a function of time (see Figure 7). After ~1 h from the time of preparation, the nanocrystal reflections effectively disappeared, suggesting that these entities decomposed or reacted in moist air. Two possibilities exist to explain these results. Either (1) the nanocrystals are embedded in the wall structure of the growing mesophase or (2) they are admixed with the mesophase at time of deposition. Since there seems to be an inverse relationship between the time dependence of the intensities of the low- (mesophase) and high-angle (nanocrystal) reflections, it is tempting to relate the disappearance of the nanocrystal reflections to mesophase growth. However, this could be coincidental and the mesophase and nanocrystals could exist as separate phases. The slight decrease in d-spacing from 66.87 Å to 64.90 Å over the first 100 min is consistent with previously reported uniaxial shrinkage, as a result of drying.[28] The present results show how sensitive this system is to the relative humidity during both dipping and the conditioning time after the dipping process.

(25) Dag, O.; Soten, I.; Celik, O.; Polarz, S.; Coombs, N.; Ozin, G. A. *Adv. Func. Mater*. **2003**, *13*, 30.
(26) Luca, V.; Watson, J. N.; Ruschena, M.; Knott, R. B. *Chem. Mater*. **2006**, *18*, 1156.
(27) Luca, V.; Bertram, W. K.; Sizgek, G. D.; Yang, B.; Cookson, D. *Langmuir* **2008**, *24*, 10737.
(28) Crepaldi, E. L.; Soler-Illia, G. J. de A. A.; Grosso, D.; Cagnol, F.; Ribot, F.; Sanchez, C. *J. Am. Chem. Soc*. **2003**, *125*, 9770.

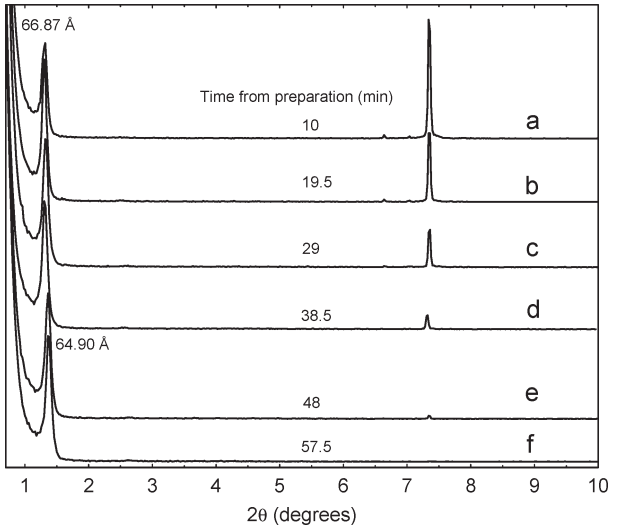

Figure 6. Variation in low-angle diffraction (reflection mode) pattern with time for B58-ZrTi-0.4 film prepared ex situ and held at 65% RH. Each pattern took 9 min to acquire. Interval between patterns was 30 s. Time at which each acquisition was started is indicated.

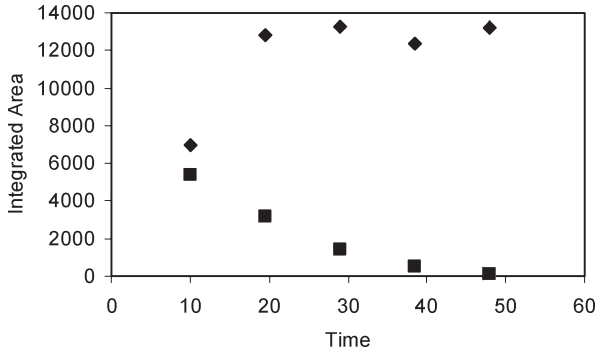

Figure 7. Variation in integrated intensity of the (◆) low-angle mesophase and (■) high-angle nanocrystal reflections, as a function of the time extracted from the data of Figure 6.

When the humidity during the B58-ZrTi-*0.4* film deposition was increased to ~70% RH in the ex situ experiments, only weak nanocrystal reflections were observed in the first 10 min, which then quickly disappeared (see Figure 8). The *d*-spacing initially increased from 64 Å to 69 Å and then progressively decreased as the film dried and contracted uniaxially, as previously described.[28] In addition to these sharp low-angle reflections, it was also possible to observe weak reflections at very low diffraction angles corresponding to a spacing of ~100 Å. The initial increase in *d*-spacing is likely to be related to the evaporation of ethanol with hydrocarbon tail protruding into the hydrophobic regions of the copolymer causing a radial redistribution. Similar expansions have been postulated to be occurring in the cetyl trimethyl ammonium bromide (CTAB)−silicate system under EISA.[29]

Characterization by TEM. TEM analysis of the B58-ZrTi-*x* (with $x = 0.2$, 0.4, and 0.8) prepared and conditioned at 65% RH, followed by heating at 200 °C, were

(29) Doshi, D. A.; Gibaud, A.; Goletto, V.; Lu, M. C.; Gerung, H.; Ocko, B.; Han, S. M.; Brinker, C. J. *J. Am. Chem. Soc.* **2003**, *125*, 11646.

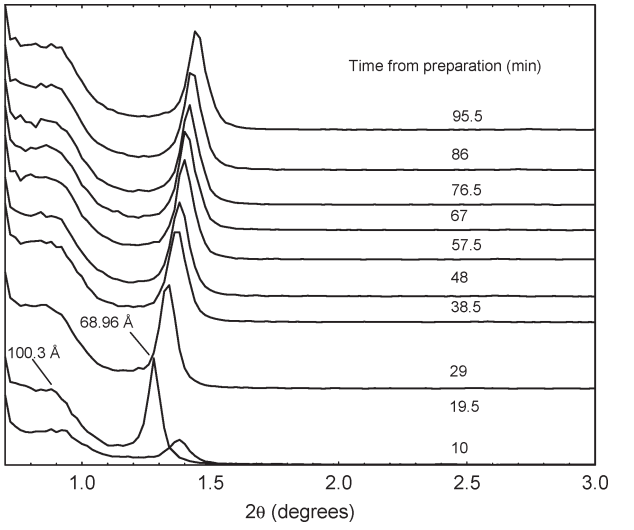

Figure 8. Variation in the low-angle (reflection mode) diffraction pattern of the B58-ZrTi-*0.4* film, as a function of time, with the humidity held constant at 70% RH. Each pattern took 9 min to acquire. Interval between patterns was 30 s.

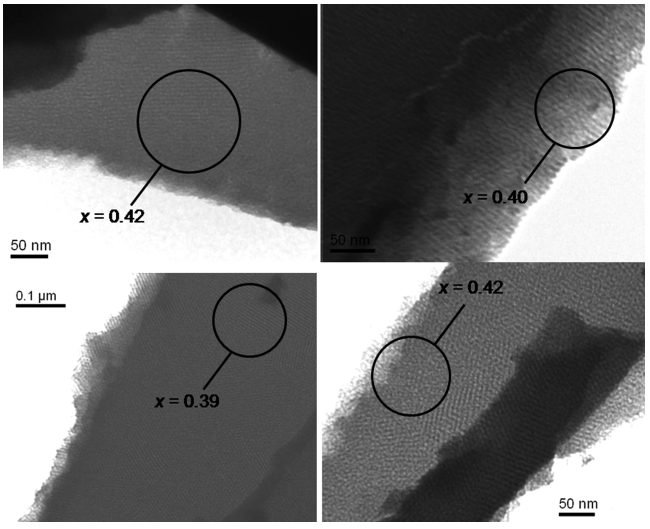

Figure 9. Selection of TEM lattice fringe images and EDS analyses of selected regions of the B58-ZrTi-*0.4* film prepared and conditioned at 65% RH, followed by heating at 200 °C. The X-ray pattern of this film was given in Figure 6.

investigated. Similarly distinctive fringes could be observed in all products, indicating the formation of well-ordered mesophases. The fringes were similar across the entire compositional range, and this supports the notion that the Zr-containing materials were similar to the sample that contained no zirconium. Importantly, the compositions analyzed by energy-dispersive spectroscopy were, within experimental uncertainty, similar to that of the precursor solution in all parts of the sample. This indicates a homogeneous dispersion of the two components on the scale of TEM observation. As an example, a selection of images and analyses is presented in Figure 9.

Characterization of Atomic Scale Mixing by EXAFS. Although the XRD *d*-spacing variations with *x* were strongly suggestive of a complete solid solution, and TEM investigation indicated that Zr and Ti were homogenously distributed on the scale of a few nanometers, this

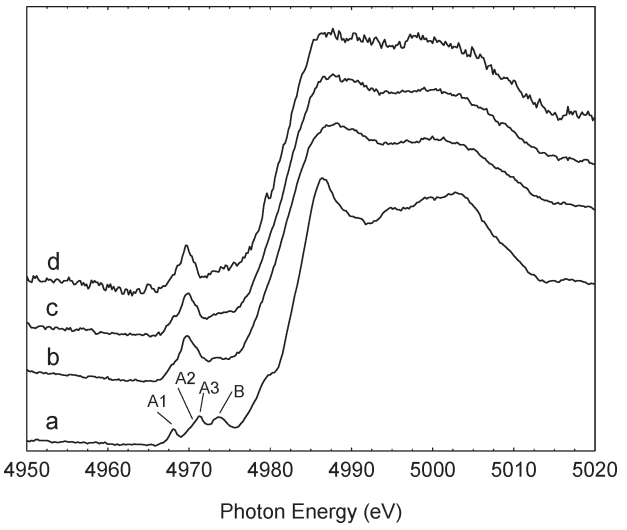

Figure 10. Ti K-edge XANES of $Zr_xTi_{1-x}O_2$−Brij58 film samples recorded at 10 K: (a) anatase, (b) B58-ZrTi-*0.2*, (c) B58-ZrTi-*0.4*, and (d) B58-ZrTi-*0.6*.

does not unequivocally prove that intimate atomic scale mixing has occurred to give Ti−O−Zr bonding. Macroscopic phase segregation into small nanoparticles remains a possibility. One way of ascertaining whether such atomic-scale mixing actually occurred was to interrogate the structure of the films using a technique that could provide direct structural atomic-scale information. For this purpose, we used X-ray absorption spectroscopy.

XANES spectra of a range of B58-ZrTi-*x* films (with $x = 0.20$, 0.40, and 0.60) are shown in Figure 10, in comparison with the XANES of nanocrystalline anatase. The pre-edge XANES of nanocrystalline anatase contains four pre-edge features, because of 4s−3d localized transitions (A1, A2, A3, and B), the assignment of which has been amply discussed previously.[22] For the present purposes, we make some simple qualitative observations. First, the A2 shoulder is difficult to discern in any of the spectra of the B58-ZrTi-*x* film samples. Second, the pre-edge of the films was less well-defined than that of bulk nanocrystalline anatase. Nevertheless, it is clear that the intense A2−A3 composite structure moved significantly to lower energies in the films, compared with anatase. Close inspection also shows that the B feature becomes less visible as the zirconium content of the films increases. The pre-edge of the film, in fact, resembles quite strongly that of amorphous titania or very small anatase nanoparticles.[22] In amorphous titania, a similar increase in A2−A3 intensity and move to lower energies has been observed and ascribed to a greater proportion of coordinatively unsaturated Ti which in turn results in a blue shift of the fundamental absorption edge as bulk semiconductor band structure is altered. It is possible to hypothesize that a similar alteration of band structure could be occurring in the films as Ti is replaced by Zr.

If Zr does indeed replace Ti in the amorphous mesopore walls to give Ti−O−Zr bonds, then this should also be reflected in the EXAFS, via an alteration in the next-nearest-neighbor coordination. That is, the transition from Ti−O−Ti to Ti−O−Zr should be readily observable.

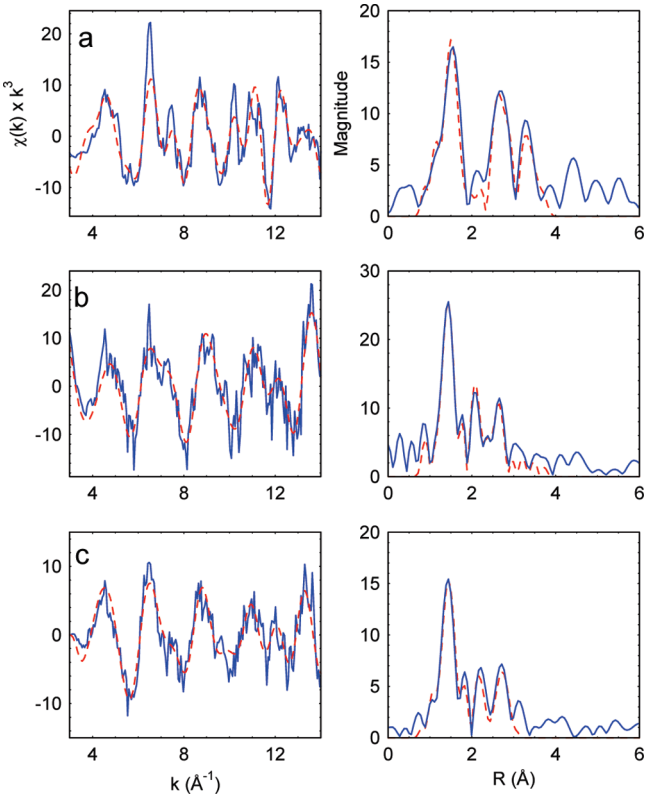

Figure 11. Ti fitted k^3−weighted Ti *k*-edge EXAFS (left) and corresponding fitted magnitude FT spectra (right) of B58-ZrTi-*x* film samples recorded at 10 K: (a) B58-ZrTi-*0.2*, (b) B58-ZrTi-*0.4*, and (c) B58-ZrTi-*0.6*.

The EXAFS spectra of the B58-ZrTi-*x* film samples are shown in Figure 11. Large differences in *k*- and R-space EXAFS of the films are apparent, as the Zr content was increased, when compared to nanocrystalline and amorphous TiO_2 materials.[22] Of all of the samples, the EXAFS of the B58-ZrTi-*0.2* film was qualitatively most similar to anatase of amorphous TiO_2 nanocrystals. However, as the Zr content increased to 0.4 and 0.6, it is obvious that significant differences appeared at longer *R* values, relative to nanocrystalline anatase or amorphous TiO_2. This observation, on its own, provides strong evidence for incorporation of scattering atoms other than Ti in the next-nearest-neighbor positions. The two Fourier transform peaks at longer distances have moved quite significantly to lower distances.

The less-than-ideal signal-to-noise ratio of the data made fitting the data less certain than it might otherwise be; therefore, fitted parameters should be treated cautiously. Nonetheless, adequate fitting of the EXAFS for these samples clearly required the addition of Zr next-nearest-neighbors to the fitting model. This seems a reasonable outcome, given the visually obvious changes occurring in the data, as a function of the amount of Zr incorporated. Such changes are particularly obvious in the R-space data that show significant modulation of outer backscattering shells. Indeed, EXAFS simulation of all of these data (see Table S1 in the Supporting

Information) was only possible if Zr was included in outlying shells, suggesting that these materials can be regarded as being homogeneous on the atomic scale. Aside from the need to include Zr in next-nearest neighbor sites, the first shell Ti−O bond length of ∼1.8 Å for the B58-ZrTi-*0.2* films, which increased to 1.89 Å for the B58-ZrTi-*0.6* films, are rather short, compared with the value of 1.95 Å for bulk anatase and rutile. However, these short Ti−O bond lengths are quite consistent with those obtained for very small TiO_2 nanoparticles, where the majority of Ti atoms are present at the surface and are undersaturated, in terms of their coordination. Such undersaturation manifests itself as shortened Ti−O/Ti−OH bond lengths, as shown by numerous previous EXAFS investigations[22,30,31] and recently supported by theoretical results.[32,33] The subject has been reviewed very recently by Luca,[34] in which a new model was proposed for small sol−gel-derived anatase nanoparticles that consisted of a core of fully saturated Ti atoms surrounded by a disordered shell of undersaturated Ti atoms. Like sol−gel anatase nanoparticles, mesoporous titania materials with high surface area and thin pore walls are also expected to contain a very large proportion of surface Ti atoms. Therefore, it is quite reasonable to expect a significant proportion of undersaturated surface Ti atoms with reduced Ti−O bond lengths, as suggested by our EXAFS results.

Detailed Examination of Reaction Mechanism Using In Situ SAXS. To provide detailed information on the self-assembly mechanism, an in situ SAXS study was undertaken, using the setup and protocol described in the Experimental Section. Detailed time-resolved studies of mesophase formation were performed in a flow-through system, using a SAXS instrument that allowed an individual dataset to be acquired within 100 s. It is important to realize that the experimental protocol used was somewhat different to that described above, during which film preparation occurred ex situ. In the SAXS experiments, the precursor solution was drawn into a vertical capillary contained within a chamber in which the temperature was precisely controlled. The precursor solution was then ejected by a regulated flow of air at controlled humidity and temperature. As the flow conditions are different to drying ex situ in quiescent air, there should be no expectation that the time scales would match those observed in the reflection SAXD (Bragg−Brentano) data described above. The data obtained in transmission using the SAXS instrument are shown in Figure 12. This data shows similar qualitative changes to those observed in the Bragg−Brentano SAXD data of Figure 6. However, it was possible to record several initial sets of data, showing only small angle

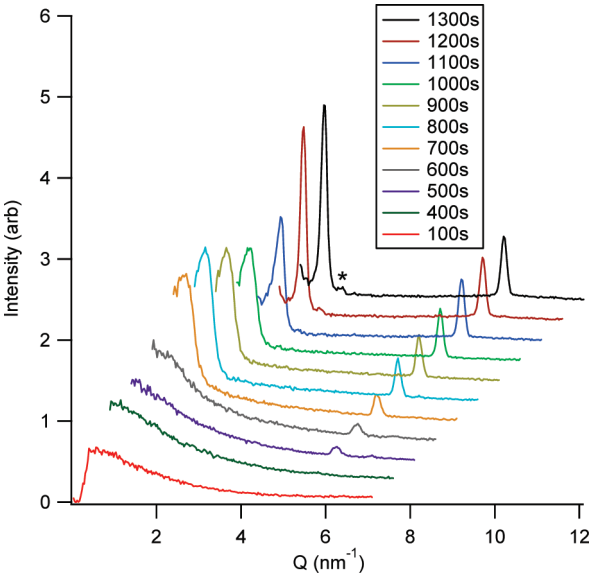

Figure 12. Fresh precursor solution (x = 0.4) 60% RH and flow rate of 8.5 mL/min. The asterisk (∗) indicates a higher-order peak.

scattering and no Bragg diffraction (data at 100 and 400 s). The first feature to appear on drying was the sharp weak high-angle due to the nanocrystals (400−500 s) and then the Bragg peak due to mesophase ordering was subsequently observed. This occurred ∼700 s after the initial film deposition. The *d*-spacing of this peak corresponds to a value of ∼97 Å and is similar to that observed at the higher humidity in Figure 8. While detailed analysis of these and other patterns will be reported in a subsequent detailed in situ SAXS study of this system, the present in situ study shows a clear sequence of events during mesophase preparation. First, low-angle scattering due to disordered building block formation, then the crystallization of these structures into well-ordered building units and then the assembly of the mesophase structure.

Discussion

The present study of zirconium titanate mesophase formation using B58 as the porogen has shown that compositionally homogeneous mixed zirconium titanium oxide mesophase materials can be prepared. This is in stark contrast with what has been observed by us in the preparation of mesoporous zirconium titanate materials with similar mole fractions of Zr where the triblock copolymer F-127 was used as a porogen.[9] In that case, neither order nor compositional homogeneity could be achieved under similar experimental conditions. Moreover, comparison of SAXD patterns of TiO_2−B58 and TiO_2−F-127 films (Figure 2) highlight the fact that mesophases with a higher degree of order are always formed for B58, all things being equal, irrespective of the relative humidity used for preparation and even after long equilibration times. These results demonstrate that relatively subtle variations in the type and number of constituents in a block copolymer can have significant implications, in terms of the properties of the materials produced.

To understand the differences in the nature of the products formed from these two amphiphiles, it is first

(30) Chen, L. X.; Rajh, T.; Jager, W.; Nedeljkovic, J.; Thurnauer, M. C. *J. Synchrotron Radiat.* **1999**, *6*, 445.
(31) Chen, L. X.; Rajh, T.; Wang, Z. Y.; Thurnauer, M. C. *J. Phys. Chem. B* **1997**, *101*, 10688.
(32) Iacomino, A.; Cantele, G.; Ninno, D.; Marri, I.; Ossicini, S. *Phys. Rev. B* **2008**, *78*, 075405.
(33) Naicker, P. K.; Cummings, P. T.; Zhang, H. Z.; Banfield, J. F. *J. Phys. Chem. B* **2005**, *109*, 15243.
(34) Luca, V. *J. Phys. Chem. C* **2009**, *113*, 6367.

necessary to first consider the chemical nature of B58 and F-127 (both being copolymers of polyethylene oxide) and any interaction that would ensue between ligands on the polymer and metal oxo-alkoxy building blocks in the solution phase, as well as perhaps the degree of hydration of the micelles formed. If the role of the block copolymers was simply the formation of an appropriate mesophase template, then the results from F-127 and B58 would be expected to be similar.

B58, or polyethylene glycol hexadecyl ether ($C_{16}E_{20}$), and Pluronic F-127 ($E_{97}P_{69}E_{97}$) are both nonionic polyoxyethylene surfactants and have the common feature that they contain ethylene oxide (E) units as the most hydrophilic element that is soluble in the selective solvent, water. However, B58 is a relatively small diblock and F-127 is a large triblock copolymer. Since the large P units in F-127 are slightly more hydrophobic than the similarly large E units in B58, it might be expected that F-127 has a lesser tendency to form micelles than B58, which also contains the hydrophilic E units coupled to a short very hydrophobic C_{16} acyl chain. In F-127, the similar E and P units can adopted tangled chain confirmations or "blobs", making for less-distinct core−shell micelles. On the other hand, the difference in hydrophilicity is expected to be more pronounced for B58 and the chains are likely to be less entangled such that the core and shell of the micelles are strongly differentiated. These factors are likely to be partially responsible for the observation of lower CMCs and greater aggregation numbers of diblock copolymers, compared with triblock copolymers.[35]

Another aspect that must be considered is the relative state of hydration of the corona/palisade regions of these two classes of amphiphile. It has recently been suggested that the difference in thicknesses of the palisade layer and corona region of these two classes of amphiphiles can be quite different. Presumably the smaller core of the B58 micelles give less PEO per unit area in the corona or shell, compared with F-127, and this allows more water to occupy the outer palisade layer. In the case of F-127, the P units give rise to a larger core and more E units per unit area in the corona, leaving less room for water. Indeed, more-solvating palisade layers are generally the case for more-conventional surfactants such as TX-100 and also diblock copolymers such as B58, compared to the corona regions of triblocks such as F-127 that are less hydrated. This probably underlies the observation of quite different solvation dynamics for water trapped in the corona and palisade regions of diblock and triblock surfactants.[36] As a result of the different extent of hydration of the corona and palisade regions, it might be expected that the ability of the triblock copolymer micelles to provide water to inorganic building units assembling through hydrolysis−condensation reactions in these regions is more limited in than that for diblock copolymers.

In a previous in situ SAXS study of the first few seconds of self-assembly in the $TiCl_4$−F-127−EtOH−H_2O system, "soft" inorganic building units were observed that could be described by two R_g values as determined from the Guinier region of the SAXS.[27] In addition, hard-sphere correlations were observed as broad Gaussian components, the *d*-spacing of which shrank over a period of hours during the evaporation process, approaching an asymptotic value of ∼1.2 nm. This was observed regardless of the ambient humidity in which the evaporation occurred. In the present $Zr_xTi_{1-x}Cl_4$−EtOH−Brij 58−H_2O system, building units of similar dimensions are also observed during the drying process and these have a similar primary *d*-spacing. However, the difference in the line width of the reflections from these similarly sized nanocrystalline building units suggests that they differ in the extent of ordering. Similar observations of nanocrystal building unit formation have been made during the preparation of other titania mesophases by Dag et al.,[25] using $C_{12}EO_{10}$, and Luca et al.,[26] using dodecyl sulfate amphiphiles. These are two quite unrelated amphiphile systems and, in both cases, the products had disordered "wormhole" mesoporosity. The present $Zr_xTi_{1-x}Cl_4$−EtOH−Brij 58−H_2O system is distinct in that we have directly observed the formation of nanocrystals in a mesophase system displaying excellent ordering characteristics. Therefore, it seems that the challenges of defining the self-assembly process in a precise manner are made stark by the range and type of building units. Therefore, we hypothesize that the more-crystalline building units observed in the $Zr_xTi_{-x}Cl_4$−EtOH−Brij 58−H_2O system are comprised of mixed-metal-oxide clusters. These are able to form because the supply of water in the palisade and corona regions of the assembling B58 micelles is close to some optimum value. Larger, more well-ordered, building units permit more ordered and conformable surfactant self-assembly. The fact that discrete building units can exist right up to the point that an ordered mesophase is formed must be important in allowing the necessary conformational flexibility, which, in turn, will depend on the interaction between these units. Of course, this internanocluster interaction is in addition to the nanocluster−PEO interaction, which must also be important in the micelle formation process. We have attempted to convey the difference between these two systems in the model presented in Figure 13, which emphasizes the greater hydration of the palisade and corona region for B58 and the differences in building units between the two systems. Note that, in the interest of schematic simplicity, the P and E units are shown in straight-chain conformation in both cases. In reality, it is quite well-known that the real structures probably involve folded chains that resemble blobs.

Little information exists in the literature regarding these internanocluster and nanocluster−surfactant interactions, since few experimental techniques can directly probe them in a rapidly evolving system. Many experimental studies have been undertaken of the adsorption of block copolymers on the surfaces of a range of

(35) Schillen, K.; Claesson, P. M.; Malmsten, M.; Linse, P.; Booth, C. *J. Phys. Chem. B* **1997**, *101*, 4238.
(36) Kumbhakar, M.; Goel, T.; Nath, S.; Mukherjee, T.; Pal, H. *J. Phys. Chem. B* **2006**, *110*, 25646.

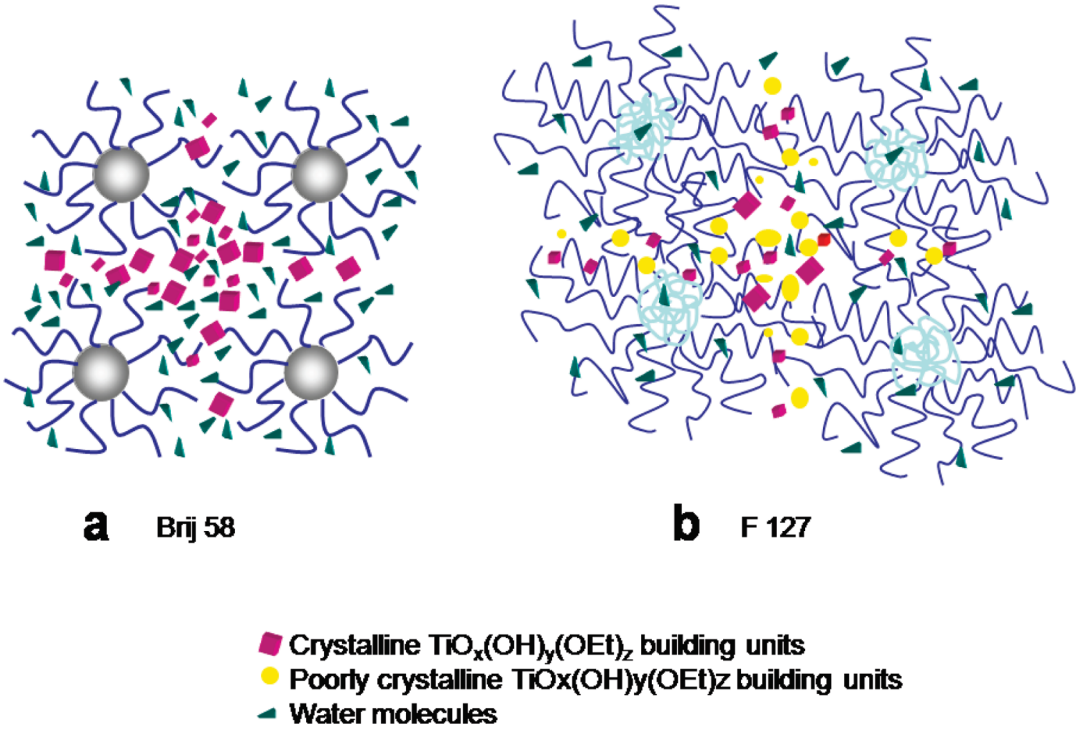

Figure 13. Model of the self-assembly processes in the case of (a) B58 and (b) F-127. Note that the E and P units are shown in schematic form and that the diagram emphasizes the greater hydration of palisade and corona regions for the B58 system.

nanostructured materials, including latex,[37] carbon,[38] silica,[39] and various other metal oxides, including layered silicates.[40] However, even in these cases, the exact nature of the interaction between metal oxides (nanoclusters or nanoparticles) and block copolymers has been difficult to glean and generally only qualitative observations of the thickness of adsorbed layers have been offered. In recent theoretical studies of nanoparticle-block copolymer systems, the interactions between block copolymers and invariant metal oxide nanoparticles has been addressed explicitly, using fairly simple potentials.[41,42] Indeed, the importance of nanoparticle−nanoparticle and nanoparticle−polymer interactions in determining the structures formed has been underscored by such studies that have been able to correctly describe experimental observations. However, unlike the case of weakly interacting but invariant nanoparticle systems, the present system poses additional challenges, because of the dynamic nature of the sol−gel hydrolysis−condensation process that is evolving over time and concomitantly influencing the macromolecular assembly. Indeed, Siperstein and Gubbins,[43] in early simulations of surfactant−inorganic(silica)−solvent systems similar to the present, restricted attention to self-assembly under "no silica polymerization conditions". Experimentally, such conditions in that system can be achieved at very low solution pH where only orthosilicate monomers are present but which, nevertheless, undergo spontaneous self-assembly without the need to remove solvent. This avoids the need to consider the time-dependent nature of the inorganic polymerization. The present system is yet more complex, because this polymerization is being driven by solvent evaporation.

A major issue to confront in this and other studies evidencing the existence of such nanocrystalline building units in mesophase preparations is the exact relationship between nanocrystal formation and the assembly of the mesophase over time. As early as 1994, Vartuli et al.[44] showed that common silicate oligomers such as D4R and the cubic octamer Q8M8 were unlikely building blocks for mesoporous silicate formation, since they did not have the required stability under the synthesis conditions (especially temperatures) typically employed. Many studies of titanate-based block copolymer self-assembly have suggested that titanate-oxo-ethoxy clusters represent the building blocks of the inorganic framework. These building blocks putatively interact with each other and also with the amphiphile molecules. Soler-Illia et al.[45] reported the preparation of dendrameric mesophase titanate materials using the previously reported so-called G1(COOH)$_6$ dendrimer and well-defined [Ti$_{16}$O$_{16}$(OEt)$_{32}$] cluster compounds. While the integrity of the cluster core under synthesis conditions was largely demonstrated by

(37) Shar, J. A.; Obey, T. M.; Cosgrove, T. *Colloids Surf., A* **1998**, *136*, 21.
(38) Lin, Y. N.; Alexandridis, P. *J. Phys. Chem. B* **2002**, *106*, 10834.
(39) Shar, J. A.; Obey, T. M.; Cosgrove, T. *Colloids Surf., A* **1999**, *150*, 15.
(40) Nelson, A.; Cosgrove, T. *Langmuir* **2005**, *21*, 9176.
(41) Sknepnek, R.; Anderson, J. A.; Lamm, M. H.; Schmalian, J.; Travesset, A. *ACS Nano* **2008**, *2*, 1259.
(42) Knorowski, C. D.; Anderson, J. A.; Travesset, A. *J. Chem. Phys.* **2008**, *128*, 164903.
(43) Siperstein, F. R.; Gubbins, K. E. *Langmuir* **2003**, *19*, 2049.
(44) Vartuli, J. C.; Schmitt, K. D.; Kresge, C. T.; Roth, W. J.; Leonowicz, M. E.; McCullen, S. B.; Hellring, S. D.; Beck, J. S.; Schlenker, J. L.; Olson, D. H.; Sheppard, E. W. *Chem. Mater.* **1994**, *6*, 2317.
(45) Soler-Illia, G. J. de A. A.; Rozes, L.; Boggiano, M. K.; Sanchez, C.; Turrin, C.-O.; Caminade, A.-M.; Majoral, J.-P. *Angew. Chem., Int. Ed.* **2000**, *39*, 4249.

^{17}O NMR, the resultant compounds did not have a well-developed ordered meso texture. The same discrete cluster compounds [$Ti_{16}O_{16}(OEt)_{32}$] were later used to make hybrid materials in the presence of the amphiphilic block copolymers PS-b-PMAA.[46] Interestingly, the resultant materials were also not ordered, despite the strong structure-directing ability of this amphiphile. In all of these studies, the signature of the cluster was deduced using ^{17}O NMR of the synthesis solution. However, this NMR technique was not applied in a quantitative manner so that no idea was given of the absolute concentration of the cluster. In other words, a two-phase system of the cluster and decomposition or hydrolysis products could easily have existed in solution, with the latter contributing to mesophase formation. Therefore, in our opinion, the entire concept of nanobuilding blocks could be flawed unless it can be proven unequivocally that the clusters do not simply act to provide feedstock for the mesophase assembly.

In the present case, the nanoclusters are clearly evidenced by XRD and, as such, a reasonable relative measure of the concentration of both mesophase and nanocluster is available. We have observed that absolute and relative intensities of nanocluster and mesophase scattering intensities are inversely correlated: the intensity of the mesophase peaks increase while those of the nanoclusters decrease, as a function of drying time at a particular humidity (see Figures 4 and 5). This correlation should not be confused with causation, because the variations in intensity could quite easily be a result of independent processes.

We have also observed that the relative intensity of the nanocluster peaks in the freshly deposited films are dependent on the aging time of the precursor solutions. This suggests that, although the clusters have reasonable stability, they do eventually decompose in solution over time.

Our more-detailed SAXS investigation of this mixed-metal system indicates strong scattering from the precursor solution at $T = 0$. This indicates that oligomeric zirconium- and titanium-containing moieties are already present in the starting solutions. As drying is initiated, the characteristic solution scattering persists only until such time that the film is visually dry. At this point, several hundreds of seconds after deposition, the nanocrystal diffraction is observed without the observation of any correlation or mesophase peak. The nanocrystal peaks then increase in intensity concomitantly with the growth of peaks due to the mesophase. In other words, both species only crystallize upon solvent evaporation and film drying. Therefore, solvent evaporation and drying clearly drive two processes: first the crystallization and then the growth of the mesophase and decomposition of the nanocrystals.

(46) Steunou, N.; Foerster, S.; Florian, P.; Sanchez, C.; Antonietti, M. *J. Mater. Chem.* **2002**, *12*, 3426.

Conclusions

We have demonstrated that using the diblock copolymer surfactant B58, it is possible, in contrast to the case for F-127, to produce well-ordered compositionally homogeneous thin films. For the first time, we have demonstrated the possibility of achieving a complete solid solution in a multicomponent oxide system, namely, $Zr_xTi_{1-x}O_2$.

It has been shown that the formation of ordered nanocrystals is composition-dependent, requiring the presence of Zr and Ti. These nanocrystals may also be present at low Zr contents; however, they achieve the order necessary to be easily detected by diffraction techniques only after x falls in the range of 0.2−0.6.

During mesophase formation, nanocrystals form first, and they then coexist with the mesophase and eventually decompose as the mesophase continues to order.

Acknowledgment. X-ray absorption experiments were supported by the Australian Research Council. Access to the Photon Factory was provided by the Australian Synchrotron Research Program, which has been funded by the Commonwealth of Australia via the Major National Research Facilities Program. The assistance of Drs. Garry Foran and James Hester with the recording of XAS data is acknowledged.

Supporting Information Available: Additional SAXD plots and a table of fitted EXAFS parameters are provided. (PDF) This material is available free of charge via the Internet at http://pubs.acs.org.